energies

MDPI

Article

Enhancing the Viability of a Promising E-Fuel: Oxymethylene Ether–Decanol Mixtures

Márton Virt and Máté Zöldy *

Department of Automotive Technologies, Budapest University of Technology and Economics, Műegyetem rkp. 3., 1111 Budapest, Hungary; virt.marton@edu.bme.hu
* Correspondence: zoldy.mate@kjk.bme.hu

Abstract: Achieving sustainable mobility is a crucial factor in maintaining long-term economic growth without adverse effects on human health and the environment. E-fuels, such as the promising oxymethylene ether (OME), can contribute to sustainable road transport. However, this compound does not meet the requirements of EN590; thus, it is unsuitable for unmodified diesel engines. This work aims to improve the applicability of OME by blending it with n-decanol, which can also be produced sustainably. Combustion and emissions were investigated in a medium-duty commercial diesel engine with different binary and ternary mixtures of oxymethylene ether, n-decanol, and B7 diesel. Laboratory analysis of six key mixture parameters revealed that the formulated blends met the EN590 requirements, with the exception of that of density. The results demonstrated that the created mixtures, including one without any diesel fuel, can be efficiently utilized in unmodified diesel engines. OME's beneficial effects on combustion and emission were preserved while its viability was improved; a maximum increase of 7.6% in brake thermal efficiency was observed, alongside a potential decrease of nearly 70% in PM emissions at unaltered NO_x levels.

Keywords: advanced fuels; oxymethylene ether; n-decanol; compression ignition engine; NO_x–PM trade-off; combustion

Citation: Virt, M.; Zöldy, M. Enhancing the Viability of a Promising E-Fuel: Oxymethylene Ether–Decanol Mixtures. *Energies* **2024**, *17*, 1348. https://doi.org/10.3390/en17061348

Academic Editor: Adam Smoliński

Received: 29 January 2024
Revised: 8 March 2024
Accepted: 9 March 2024
Published: 12 March 2024

1. Introduction

Since the Industrial Revolution, the average global temperature has risen around 1 °C. The further growth of temperature can generate irreversible changes in the ecosystem. To avoid this, 196 parties adopted the Paris Agreement to keep the temperature rise compared to the preindustrial levels well below 2 °C [1]. This agreement is the basis of many new regulations, such as the Fit for 55 package of the European Union (EU). The EU is devoted to achieving climate neutrality by 2050, and the aforementioned package contains proposals to cut greenhouse gas emissions until 2030 by at least 55% compared to the 1990 level [2]. Due to these ambitious goals, the EU decided that vans and passenger cars manufactured after 2035 cannot be equipped with internal combustion engines unless they rely on e-fuels [3]. Battery electric vehicles are a great solution for cutting the emissions of passenger cars. However, this technology has many demerits that hinder its effective application in various transportation sectors. Aside from the high price of materials, the long charging time, and the low durability of batteries, energy density is the main issue. Even the best state-of-the-art research batteries have an energy density of only around 2 MJ/kg [4]. Compared to the energy density of liquid fuels (around 40 MJ/kg), this shows that battery electric technology is not competitive in sectors requiring high energy density. Therefore, aviation [5], sailing [6], and road transport [7] require the development of climate-neutral advanced fuels.

These fuels can be e-fuels or waste-based biofuels. The former refers to synthetic fuels produced with green electricity, such as the widely investigated oxymethylene ether (OME) [8]. The latter refers to fuels created through biological processes, such as n-decanol, which we use in this work to improve the applicability of OME. The biomass starting

material is crucial in achieving climate neutrality in both cases due to the carbon cycle [9]. Shortly, the CO_2 generated from biomass is consumed by plants, which will later form biomass again. However, feedstocks that cause direct or indirect land-use changes can eliminate the benefits of the carbon cycle; thus, the best biological feedstock is waste [10]. In the case of e-fuels, green electricity is another critical factor. On the system level, renewable energy is converted into chemical energy, which is stored in fuel. However, a significant challenge with e-fuels is the typically low energy efficiency of the production process chain. This issue may pose viability concerns, necessitating the exploration of appropriate solutions. It is noteworthy that despite the inherent inefficiency in the production process, e-fuels are unavoidable in numerous sectors due to their high energy density and climate neutrality. Fortunately, there are advances in the effectiveness of e-fuels. Researchers recently demonstrated an outstanding 73% process chain efficiency in the case of OME [11].

Heavy-duty vehicles for road transport use compression ignition engines, and among the many promising diesel alternatives [12–14], OME is one of the most investigated. Regarding current research activities, the authors of [15] analyzed the origin and number of papers published on OME and found that extensive research began after 2015; nowadays, the interest is still ongoing. The top three countries that lead the research in this field are China, the US, and the UK. OME is an oligomeric compound with a molecular structure of CH_3-O-(CH_2-O)$_n$-CH_3, where n defines the degree of polymerization or, in other words, the chain length. The degree of polymerization highly influences the physicochemical properties [16]. Table 1 presents the main properties of OMEs with different chain lengths compared to the EN590 [17] requirements. As the chain length increases, the cetane number (CN), density, viscosity, and oxygen content also increase. The CN can reach values well above 80, and nearly half of the molecule's mass can be attributed to oxygen. The density is higher and the viscosity is lower than the requirements of EN590. The main changes in the engine's behavior can be attributed to the extremely high cetane number and oxygen content. These effects can be observed in the cases of other similar oxygenates, such as diethyl ether [18].

Table 1. Properties of OMEs with different degrees of polymerization [19].

Property	EN 590	OME_1	OME_2	OME_3	OME_4	OME_5	OME_6
Lower heating value [MJ/kg]	-	23.3	21	19.6	19	18.5	17.7
Cetane number [-]	>51	28	68	72	84	93	104
Density at 15 °C [kg/m^3]	820–845	860	980	1030	1070	1110	1140
Kinematic viscosity at 40 °C [mm^2/s]	2–4.5	0.37	0.559	0.866	1.33	1.96	n.i
Boiling point [°C]	-	42	105	156	202	242	273
Flashpoint [°C]	>55	−32	12	54	88	115	169
Oxygen content [wt%]	-	42.1	45.2	47	48.1	48.9	49.5

OME can be produced through multiple methods. If OME is produced via the e-fuel route, the process starts with syngas, consisting of H_2, CO, and CO_2. This is mainly produced from biomass feedstock through gasification. After CO_2 removal and adjustment of the H_2–CO ratio, a catalytic reaction can produce methanol and formaldehyde. Using these compounds and water, OMEs with different chain lengths can be formed [20]. The resulting fuel can be carbon neutral due to the carbon cycle of the biomass feedstock and the green electricity that provides the energy for OME production. Biomass is not the only possible feedstock, as CO_2 from direct air capture can also be used [21].

From practical perspectives, OME's high CN reduces the ignition delay (ID); thus, the combustion pressure gradient decreases. The compound's volatility is also high, and this also contributes to the enhanced combustion of OME [22]. Another effect on the combustion is that it becomes shorter due to the accelerating effect of the oxygen present in the fuel. This shorter duration of combustion (DoC) can lead to increased efficiency. There are also many changes regarding the emissions. Due to multiple aspects, the particulate matter

(PM) emissions with OME become very small. The main reason is the high oxygen content, which reduces soot formation. In addition, the absence of C-C bonds and the high hydrogen concentration also help to cut soot formation [16]. Regarding safety, OME is non-toxic, and with longer chain lengths, the flashpoint also meets the requirements of EN590.

It is clear that the compound has major benefits, but it also has some serious demerits. OME's lower heating value (LHV) is nearly half that of mineral diesel, and due to its strong polarity, the molecule is incompatible with conventional fluorocarbon elastomers (such as FKM) that are commonly used in fuel systems [23]. Both issues are related to the high oxygen content. The high density and the low viscosity also limit the applicability of neat OME in unmodified engines. Furthermore, OME is nonbiodegradable, which causes it to pose environmental risks, and its high vapor pressure makes the escape of vapor from the tank possible [24]. The molecule's C-O bonds, methyl groups, and formaldehyde structures can contribute to higher carbon monoxide, methane, and formaldehyde emissions during extensive exhaust gas recirculation (EGR) [16]. The oxygen content can also lead to increased NO_x emissions; however, this can be compensated with exhaust gas recirculation [25].

The disadvantages of OME can be suppressed by mixing it with other fuels. Many studies have investigated OME blends with conventional diesel fuel or biodiesels from different feedstocks. In future fuels, mineral diesel should not be used, and biodiesels have many problematic properties. Therefore, this work presents a new and better approach. Alcohols have been the focus of advanced fuel research for a long time due to their many benefits. Due to their diesel-like properties, long-chain alcohols can be applied in large ratios in compression ignition engines. One such long-chain alcohol is n-decanol, a straight-chain fatty alcohol with ten carbon atoms. Its CN and LHV are somewhat lower than diesel's. The density meets the EN590 criteria, but the viscosity is much higher than what is required. This compound is rarely investigated as a fuel, but some previous works proved its beneficial application for compression ignition engines [26]. Researchers demonstrated that the thermal efficiency can be increased, and the PM, hydrocarbon (HC), and CO emissions can be decreased with n-decanol blends [27]. Researchers experienced increasing [28] and decreasing [29] brake specific fuel consumption (BSFC) as well; thus, it depends on the conditions of the application. It can be concluded that some positive effects of the oxygen content can be observed in the literature, but the negative effects are not detrimental, since n-decanol has much less oxygen than OME does.

n-decanol can be sustainably produced from non-food feedstocks [30]. A typical biological approach to n-decanol production is to use Escherichia coli [31]. This Gram-negative enteric bacteria can produce n-decanol and other long-chain alcohols as a volatile metabolite. The production rate can be increased with the addition of fatty acids. An alternative approach for biological production uses genetically modified Yarrowia lipolytica [32]. If a specific enzyme of this oleaginous yeast is expressed, then n-decanol can be produced in low quantities. The production of n-decanol and other alcohols can be increased after deleting a specific gene.

By comparing the properties of the two compounds, it can be presumed that the bad properties of OME and n-decanol can compensate for each other, and mixtures close to the requirements of EN590 can be formed. Both compounds can be sustainably produced; thus, OME–decanol mixtures are expected to be excellent fuel alternatives with low environmental impacts and good applicability in compression ignition engines. Therefore, to prove these assumptions, this study investigated the emissions and combustion of novel OME–decanol mixtures at three loads with a constant speed of 1400 rpm. As a supplementary investigation, the fuels' compatibility with FKM sealings was also studied.

2. Materials and Methods

2.1. Test Fuels

This work investigated four OME–decanol mixtures and compared their performance with that of neat B7 diesel. The first three mixtures also contained B7 diesel with a de-

creasing ratio, while the last was only made from OME and n-decanol. All three blending components were commercially available. The OME_{3-5} mixture was applied for this investigation, since this chain length range is widely used in engine tests. The OME_{3-5} mixture that was used contained more than 85 wt% of OME with a chain length between 3 and 5. The purchased n-decanol's purity was over 98%.

A detailed laboratory analysis was applied to the pure compounds and the four mixtures to measure six fundamental properties. Karlsruhe Institute of Technology is a pioneer in OME research [33], and the laboratory analyses were carried out with their kind assistance. The measured properties of the blending components can be seen in Table 2. The densities were measured with a simple gravimetric method. The viscosities were measured with a Cannon–Fenske viscosimeter [34]. The indicated cetane numbers (ICNs) were measured with an AFIDA analyzer according to DIN EN 17155 [35]. The advantage of this method is the small sample amount (50 mL). However, it should be noted that the ICN is not exactly the CN. The lubricities were measured with a high-frequency reciprocating rig (HFRR) according to DIN EN ISO 12156 1 [36], and the wear scar diameters (WSDs) were reported. The LHVs were determined with an IKA C 5000 (by IKA-Werke, Staufen, Germany) calorimeter, and the flash points were measured according to ASTM D 7094 [37]. The oxygen concentration was the only non-measured parameter. For the B7 fuel, an oxygen content of 1 wt% was assumed based on previous experiences, and for OME and n-decanol, the molecular structure was used to calculate it.

Table 2. Measured properties of the pure blending components.

Fuel	B7	OME_{3-5}	n-Decanol	EN590
Density at 15 °C [kg/m^3]	844.2	1063.2	832.6	820–845
Kinematic viscosity at 40 °C [mm^2/s]	2.780	1.163	6.910	2–4.5
Oxygen concentration [wt%]	~1.00	47.73	10.11	-
Indicated cetane number [-]	52.7	76.9	46.7	>51
WSD at 60 °C [µm]	190	440	390	<460
Lower heating value [MJ/kg]	45.55	21.93	41.85	-
Flash point [°C]	67	50	112	>55

It is discernible that OME_{3-5} had a much higher density and much lower viscosity than the EN590 criteria. Its LHV was too low, but the oxygen content and the CN were outstandingly high. n-decanol had a proper density, while its viscosity was too high. The LHV and the CN could be considered good. The flashpoint and the WSD met the EN590 requirements for both compounds. From these properties, it could be assumed that the OME–decanol mixtures were able to meet the requirements of EN590, except for the density.

In our previous work, we designed four mixtures that were close to the EN590 requirements [38], and they were created and applied for the current research. Their properties are demonstrated in Table 3. The resulting blends were very promising. As expected, the density was the only property that did not meet the requirements of EN590. This could negatively affect the engine behavior due to the volumetric fuel injection; however, the difference was marginal. The resulting viscosities were in the center of the required range, and the flashpoints were also high enough. Interestingly, the WSD exhibited a highly nonlinear correlation with the mixture composition; however, all blends demonstrated good lubricity. The LHVs could be considered good, but as the oxygen content of the mixtures increased, their values decreased. The indicated cetane number was similar to that of B7 diesel in all cases; however, D70-O30 had a slightly smaller ICN due to the high n-decanol content. Overall, the fuels could be safely tested in an engine. It should be noted that OME can damage polar sealings in the long term; thus, the application of alternative sealing materials should be considered. Due to the short measurement times, our test engine remained unmodified, and we did not experience any harmful effects on the fuel

system. Regarding the stability of the mixtures, there were no miscibility problems. Even after several months of storage, phase separation did not occur in the leftover samples.

Table 3. Measured properties of the created binary and ternary mixtures compared to the EN590 requirements.

Fuel	D10	D30-O10	D50-O20	D70-O30	EN590
B7 content [vol%]	90	60	30	0	-
1-decanol content [vol%]	10	30	50	70	-
OME3-5 content [vol%]	0	10	20	30	-
Density at 15 °C [kg/m^3]	842.3	851.4	863.2	898.0	820–845
Kinematic viscosity at 40 °C [mm^2/s]	3.23	2.90	2.93	2.99	2–4.5
Oxygen concentration [wt%]	1.09	8.87	16.31	23.42	-
Indicated cetane number [-]	53.2	54.1	54.4	51.1	>51
WSD at 60 °C [µm]	430	170	160	160	<460
Lower heating value [MJ/kg]	45.18	41.53	38.14	34.82	-
Flash point [°C]	69	64	64	68	>55

2.2. FKM Compatibility Test

As mentioned previously, the application of OME can be problematic for unmodified engines because this compound is incompatible with the FKM sealing materials that are commonly used in engine fuel systems. Thus, material compatibility issues had to be addressed before conducting engine dyno tests. To determine the effects of the applied fuels, small FKM O-rings were introduced into test tubes containing 10 mL of the mixtures outlined in Table 3, as well as the individual blending compounds specified in Table 2. The dimensions and masses of the O-rings were recorded both prior to and following a continuous immersion period of 5 days. The reported weights were determined with a Mettler Toledo EL204-IC (by Mettler Toledo, Columbus, OH, USA) analytical balance with a resolution of 0.1 mg. The sealings' geometry was measured with a Keyence VR-5000 3D measurement system (by Keyence, Mechelen, Belgium) with a precision of ±2 µm. The inner and outer diameters were determined with the "best fit" method of the system, which was capable of automatically finding the edges of the measured components. It was assumed that the O-rings were ideal toruses, so the diameters were used to calculate the tube radius and the radius of revolution. From these parameters, the volume of the torus could be derived with the following formula:

$$V = 2\pi r^2 R^2, \quad (1)$$

where r is the tube radius and R is the radius of revolution.

2.3. Engine Dyno Measurement Setup

The experiment was carried out on a Cummins ISBe 170 30 (by Cummins Inc., Columbus, OH, USA) turbocharged, medium-duty commercial diesel engine that was used for many previous studies [19,39,40]. The engine was equipped with a common-rail injection system, an intercooler, and a high-pressure (HP) and low-pressure (LP) EGR system, and it was installed on an engine dynamometer. The temperature and pressure could be measured at the intake side before and after the compressor and after the intercooler. The exhaust side also had measurement points before and after the turbine and at the exhaust outlet. The fuel consumption was measured with an AI 2000 gravimetric device (by Energotest, Dunaharaszti, Hungary). Table 4 presents the engine's main parameters.

Table 4. Properties of the Cummins ISBe 170 30 engine.

Parameter	Specification
Engine displacement	3922 cm^3
Bore	102 mm
Stroke	120 mm
Compression ratio	17.3
Rated effective power	125 kW

The EGR rate could be varied with the HP- and LP-EGR valves and the exhaust brakes. These EGR systems are shown in Figure 1. Through the measurements, only the HP-EGR valve was used. The valves could be controlled via CAN communication with a dSpace MicroAutoBox DS1401/1505/1506 (by dSpace, Paderborn, Germany) and the sensor data were also transmitted via CAN. The combustion analysis was realized with an AVL indicating system. The cylinder pressure was measured with an AVL GH13P (by AVL List, Graz, Austria) piezoelectric sensor with a linearity of ±0.3% FSO. The sensor was connected to the seat of the glow plug. An AVL 365C (by AVL List, Graz, Austria) crank angle encoder with 0.1 °CA resolution was used to determine the crankshaft position. The indicating data were processed with an AVL 612 Indi-Smart (by AVL List, Graz, Austria), which was an 8-channel multipurpose indicating device; thus, it also had charge amplifiers for the piezoelectric sensors. AVL IndiCom (by AVL List, Graz, Austria) was used to process the combustion data, and the engine measurements were automated with a Matlab/Simulink model that could control the engine and the dyno via CAN. The oxygen and NO_x concentration could be measured with a UniNOx-Sensor (by Continental, Hannover, Germany) with an accuracy of 10 ppm. To assess the opacity of the exhaust gas, an AVL 439 opacimeter (by AVL List, Graz, Austria) with 0.1% sensitivity was applied. The emissions were not treated with catalysts or with a diesel particulate filter.

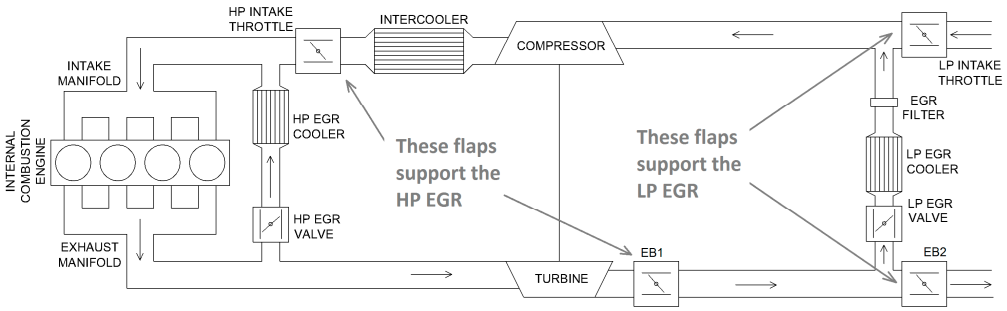

Figure 1. Airpath system of the test engine [41].

2.4. Engine Dyno Test Methods and Calculations

Two engine dyno tests were performed utilizing the formulated mixtures across constant low, medium, and high loads. Based on the engine's typical operational profile and our prior research, 100, 200, and 300 Nm loads were used at 1400 rpm. The first test investigated the NO_x–PM compromise at a high load by varying the EGR valve position from 0 to 100%, and the results are presented in Section 3.2. The second test investigated the engine economy and combustion across the 3 aforementioned constant loads. To minimize the influence of extraneous variables, EGR was not applied in this experiment. The BSFC and brake thermal efficiency (BTE) results are reported in Section 3.3. Section 3.4.1 presents the most important combustion-related parameters: the peak combustion pressure gradient (dp_{max}), start of combustion (SoC), and DoC. The reported values are the averages of the measured duty cycles after conditioning. Section 3.4.2 examines the heat release rates (HRRs) in this experiment under low- and high-load conditions. Since all blends exhibited similar combustion behavior, the medium-load curves were omitted as they do not contribute additional information.

Several standard calculation methods that were also used in our previous experiments were applied [19]. The NO_x, PM, BSFC, and BTE results were specified to the normal power, which the following formula was used to calculate:

$$P_{norm} = P_{eff} \cdot \frac{p_0 - \phi_0 \cdot p_{g0}}{p_{amb} - \phi_{amb} \cdot p_{g,amb}} \cdot \sqrt{\frac{t_{amb} + 273}{t_0 + 273}}, \quad (2)$$

where P_{eff} is the effective power, p_{amb}, t_{amb}, and ϕ_{amb} are the ambient pressure, temperature, and humidity, p_0, t_0, and ϕ_0 are the pressure, temperature, and humidity under normal conditions, and p_g is the vapor pressure of water. Then, the BSFC is

$$\text{BSFC} = \frac{\dot{m}_{fuel}}{P_{norm}}, \quad (3)$$

where $\dot{m}_{fuel}$ is the fuel mass flow. Then, the BTE can be derived as follows:

$$\text{BTE} = \frac{1}{BSFC \cdot LHV}, \quad (4)$$

where LHV is the lower heating value of the mixture. The pressure gradient was determined from the measured cylinder pressure. This pressure was also used to calculate the heat release rate with the First Law of Thermodynamics [42]:

$$\frac{dQ_b}{d_\phi} = \frac{\kappa p}{\kappa - 1} \cdot \frac{dV}{d_\phi} + \frac{V}{\kappa - 1} \cdot \frac{dp}{d\phi} - \frac{dQ_w}{d_\phi}, \quad (5)$$

where Q_b is the released heat, κ is the adiabatic gas constant of air, p is the pressure in the combustion chamber, V is the volume of the combustion chamber, Q_w is the heat loss, and ϕ is the crank angle. The heat loss was neglected during our calculations. The SoC was the crank angle at which 5% of the heat was released. The level of 90% heat release marked the end of combustion. The DoC was the difference between the two previous crank angle values.

The measured NO_x concentration was converted into brake specific NO_x emission with the exhaust mass flow rate and the normal power. The intake mass flow rate and fuel consumption were measured, so the exhaust mass flow rate was estimated to equal the sum of these. The PM emission was derived from the measured opacity according to the methods described in [43]. At first, the filtered smoke number was derived from the opacity; then, the smoke concentration could be determined. The PM emissions could be calculated from this concentration and the exhaust flow rate.

3. Results and Discussion

3.1. Compatibility with FKM Sealing Materials

Firstly, the results of the material compatibility assessments are presented. The dimensions and masses of the seven FKM O-rings were measured prior to and after the test. The original average mass of the O-rings was 63.29 mg with a standard deviation of 0.79 mg, while the average volume was 31.74 mm^3 with a standard deviation of 0.56 mm^3. Table 5 shows the resulting mass and volume deviations compared to the original mass of each O-ring after 5 days of immersion in the fuels. As expected, neat B7 did not have any considerable effects on the sealings. The results showed that n-decanol behaved similarly; thus, it was also compatible with the FKM sealings. However, pure $OME_{3\text{-}5}$ had a significant impact on the O-rings. The weight increased by 56.69%, and the volume increased by 106.38%. Since OME is strongly polar, the polar FKM molecules attracted OME; thus, it permeated the sealing and resulted in swelling. Note that the density of the O-ring decreased. This was logical because the FKM rubber had a higher density (~2000 kg/m^3), and $OME_{3\text{-}5}$, with its lower density, resulted in an overall diminution. These major effects made neat $OME_{3\text{-}5}$ unsuitable for safe application in unmodified engines. Regarding the

mixtures, D10 did not have any influence on the sealings, since it does not contain any OME_{3-5}. The other samples showed signs of OME permeation, which increased with the OME concentration. The D70-O30 blend exhibited a 22% increase in weight and a 41.87% increase in volume.

Table 5. Mass and volume deviations of the FKM O-rings after 5 days of immersion.

Fuel	Δm [mg]	Δm [%]	ΔV [mm^3]	ΔV [%]
B7	0.3	0.48	−0.88	−2.75
OME_{3-5}	36	56.69	33.76	106.38
n-decanol	0.5	0.78	−0.64	−2.01
D10	0.7	1.11	−0.54	−1.68
D30-O10	5.2	8.10	4.83	14.75
D50-O20	9.3	15.20	8.42	27.41
D70-O30	14.1	22.00	13.42	41.87

Our test engine's fuel system was unmodified; however, it was concluded that the blends could be safely tested. Figure 2 presents some of the O-rings before and after the compatibility assessment. Blends with lower OME concentrations are not included in the figure because their very small geometrical changes were hardly visible. It was clear that the application of neat OME_{3-5} would be problematic; however, the geometric changes of D70-O30 and the other blends were not detrimental. The duration of the engine dyno tests was short; thus, the blends were only present in the fuel system for several hours. Moreover, the fuel's contact with the sealings was not as direct as during the compatibility test. Considering these conditions and the proper physical properties of the blends, the engine dyno tests could be safely performed.

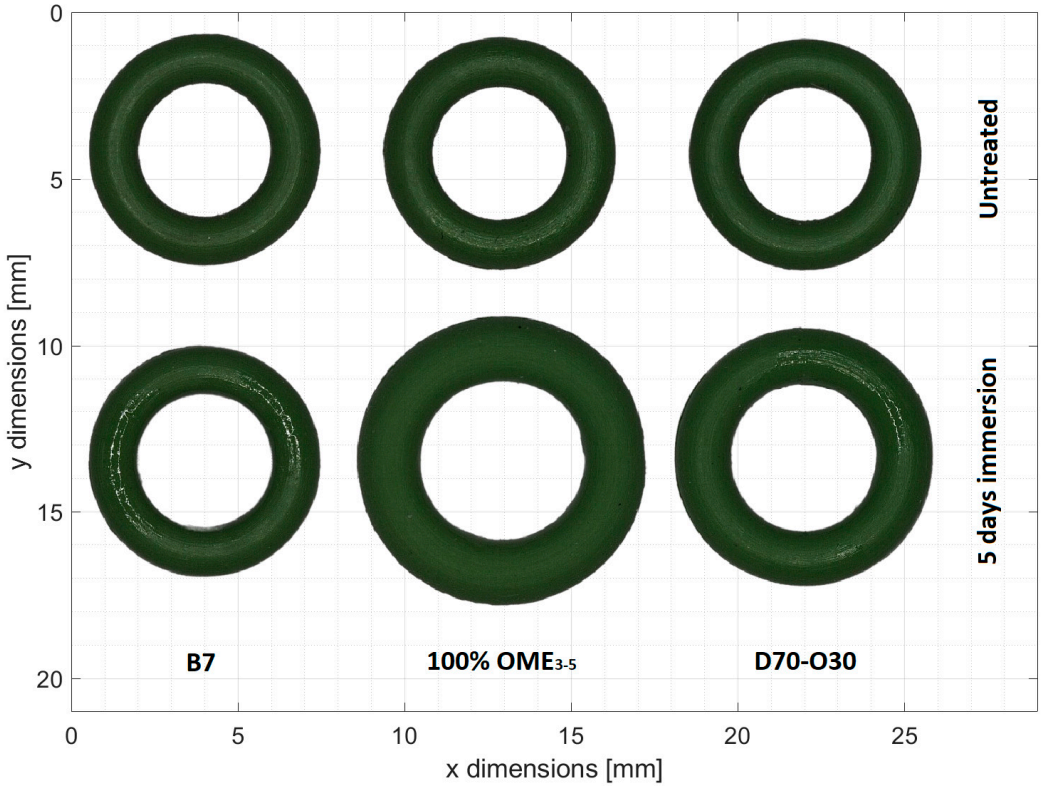

Figure 2. Comparison of FKM O-rings before and after 5 days of immersion in neat B7, OME_{3-5}, and the D70-O30 mixture.

3.2. Emissions

In the case of diesel engines, NO_x and PM emissions are the most problematic; thus, this work focuses on these. NO_x emissions are mainly generated through the Zeldovich mechanism [44], which requires high temperatures and oxygen-rich air. High temperatures reduce PM emissions since the generated soot can burn more efficiently during combustion. Among other aspects, this is the reason for the existing NO_x–PM trade-off in conventional diesel engines. However, this trade-off can be improved by employing advanced fuels, especially oxygenates, leading to a more favorable emission compromise. Oxygenates help to reduce PM emissions by suppressing soot generation. The oxygen content of a fuel can also increase NO_x emissions. Still, the change is usually marginal given that oxygen molecules in the air primarily contribute to the oxidation of nitrogen [45]. Figure 3 demonstrates the NO_x–PM trade-off resulting from various EGR positions with the tested fuels. It is discernible that the increasing oxygenate content improved the trade-off. D10 had no significant effects, but for D30-O10, the curves were much better than those for pure B7 diesel. As described before, the main reason for this improvement was the high oxygen content. D10 had a comparable oxygen ratio (1.09 wt%) to that of B7 (1 wt%), but the other blends exhibited significantly higher oxygen levels. Our previous research with B7–OME blends [19] and that of other researchers [16,24] also concluded that the trade-off significantly improved with oxygenates, and it appeared that the behavior was the same with OME–decanol mixtures.

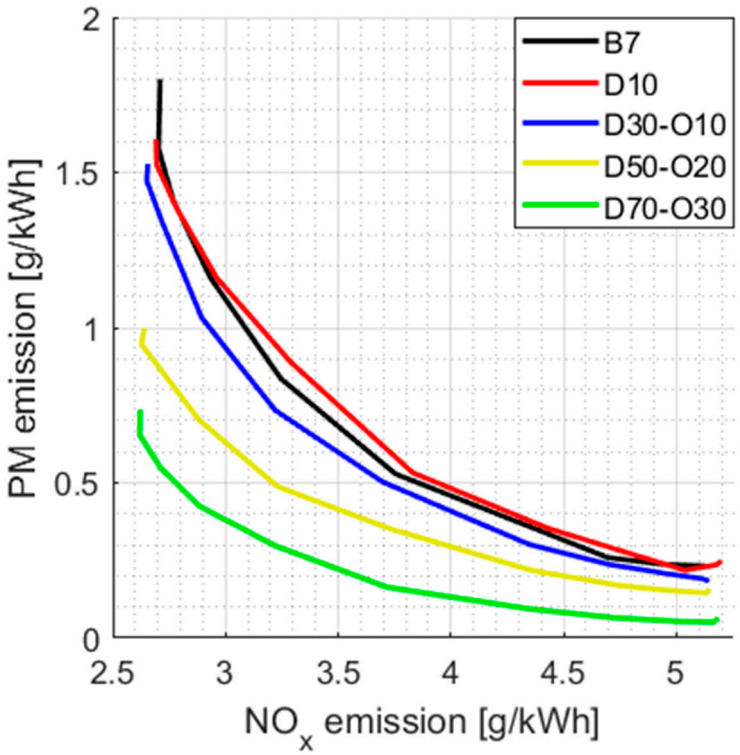

Figure 3. NO_x–PM trade-off at 1400 rpm and a load of 300 Nm with the different fuels.

3.3. Economy

The BTE can describe the engine economy well, as it includes all engine losses. The engine's original BTE was around 28% with B7 diesel at the investigated loads. With the new fuels, an improvement was expected because our previous studies [19] and other works [46] demonstrated that OME enhances the BTE. This effect was primarily attributed to the high oxygen content of OME, which enhanced the combustion efficiency. Furthermore, oxygen accelerates combustion, thereby reducing the DoC, which, in turn, positively impacts the BTE. While n-decanol contains less oxygen, a similar effect could be anticipated when it was present in a high blending ratio within the mixtures. Figure 4 presents the BTE with

the applied fuels. As expected, the BTE showed an increasing tendency as the oxygenate ratios rose in the mixtures. The most clear improvement could be seen at higher loads. This was explained by the fact that oxygen's combustion-accelerating effect was exposed chiefly during the diffusion flame period, which was the dominating combustion phase at high loads. At small loads with lower oxygenate blends, the change in the BTE was marginal; however, D70-O30 still greatly improved the efficiency. It could also be observed that the D10 mixture decreased the BTE at small loads. According to Table 3, this mixture had a notably higher viscosity than that of the other blends, although it still complied with the EN590 standard. The higher viscosity resulted in deteriorated spray atomization, negatively impacting its efficiency. Hence, this could be the primary reason for the poor performance of D10.

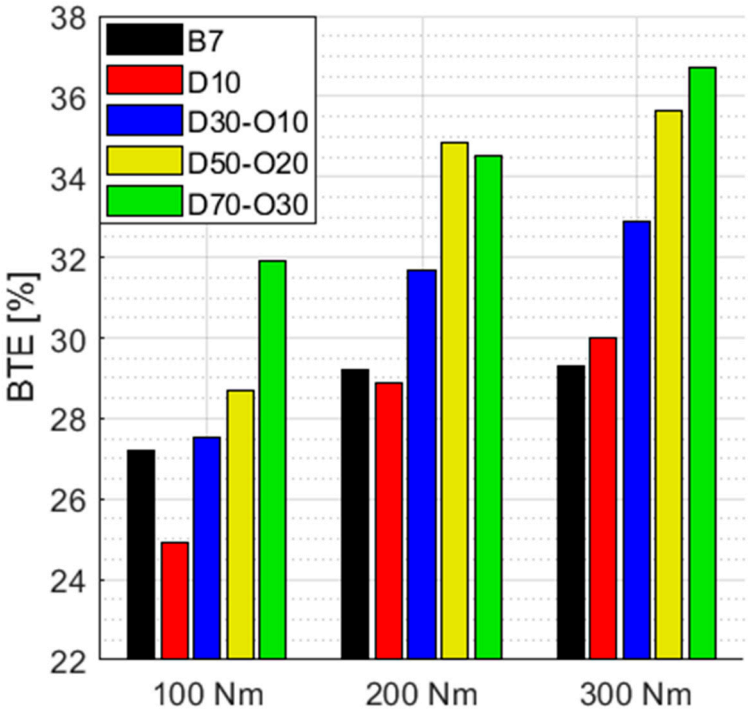

Figure 4. Brake thermal efficiency with the tested fuels at 1400 rpm and different loads.

The other important economy-related parameter is the BSFC. This is mainly affected by the LHV and the BTE. An increased oxygen content of fuel reduces the LHV [22], which leads to higher fuel consumption; thus, bigger fuel tanks may be needed. Figure 5 shows the BSFC achieved with the tested fuels. The foreseen increasing tendency could be observed, especially at low loads and for the D70-O30 blend. At 200 and 300 Nm, the enhanced BTE could effectively compensate for the smaller LHV; thus, the BSFC did not rise there significantly. The only exception was the D70-O30 mixture, which had an LHV so small that even the outstanding BTE could not reduce the BSFC much. From the economy-related results, the high oxygenate content proved to be beneficial due to the improvement of the BTE, but the fuel price per mass could also affect the optimal composition.

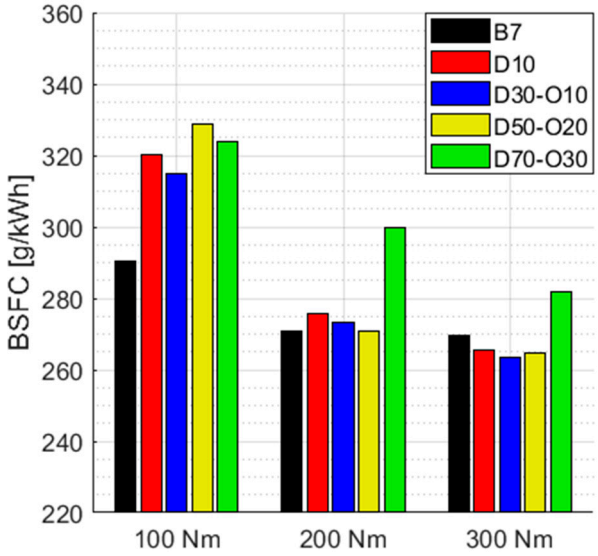

Figure 5. Brake specific fuel consumption of the tested fuels at 1400 rpm with different loads.

3.4. Combustion

3.4.1. Mean Combustion Properties

The compounds' effects on combustion also needed to be beneficial for safe engine application. The first investigated parameter was the peak combustion pressure gradient, which is presented in Figure 6. To avoid engine damage, this parameter must be under an upper limit—usually, 6 bar/°CA for commercial diesel engines [47]. The pressure gradient remained under this limit for all of the measured points. The highest values appeared at 100 Nm because, here, the premixed flame was dominant, and it was characterized by fast heat release. Higher cetane numbers resulted in shorter ID; thus, the premixed combustion phase decreased, and the heat release rate was diminished. This could partially explain the characteristics experienced at 100 Nm; however, D70-O30 also performed better than B7 despite the smaller measured ICN. At 300 Nm, the effect of the oxygenates changed. Here, the diffusion flame was dominant, and the higher oxygen content of the blends accelerated the combustion. This increased rate of heat release resulted in higher pressure gradients. However, this was not a problem, since the upper limit was still much further than for lower loads.

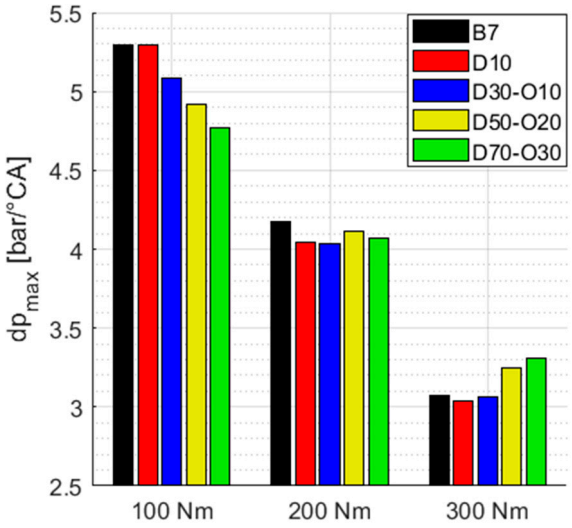

Figure 6. Peak combustion pressure gradient of the tested fuels at 1400 rpm with different loads.

Next, the start of combustion is demonstrated in Figure 7. The effects of the compounds were clear. The combustion started earlier; however, the extent of the change was small. This was the result of the drop in ID due to the better ignitability. The easy vaporization of OME could also contribute to the advanced SoC.

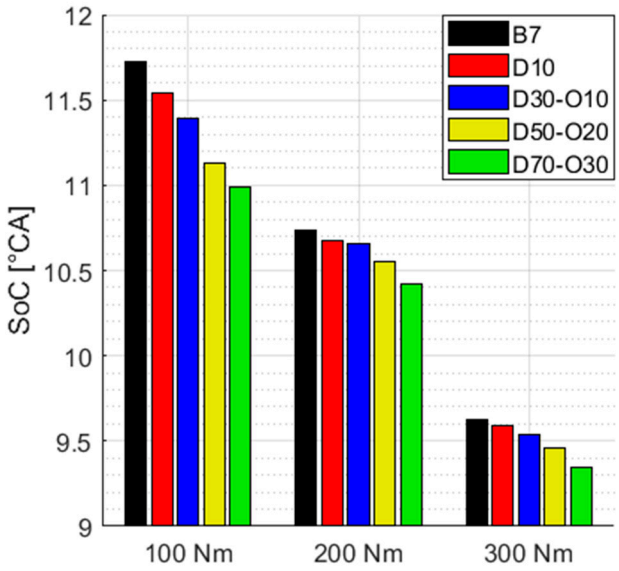

Figure 7. Start of combustion of the tested fuels at 1400 rpm with different loads.

Figure 8 demonstrates the changes in the duration of combustion. The results of the 100 Nm load fit very well with those of the BTE presented in Figure 4. D10 somewhat increased the DoC, which resulted in a lower BTE, while the mixtures with decreased DoC generated a better BTE. The 200 and 300 Nm results showed similar tendencies: Only mixtures with higher OME concentrations had significant influences. These mixtures had the most oxygen; thus, they had the strongest combustion-accelerating effects. The amount of DoC diminution was similar to the decrease that occurred in [19,48] with OME and B7 mixtures.

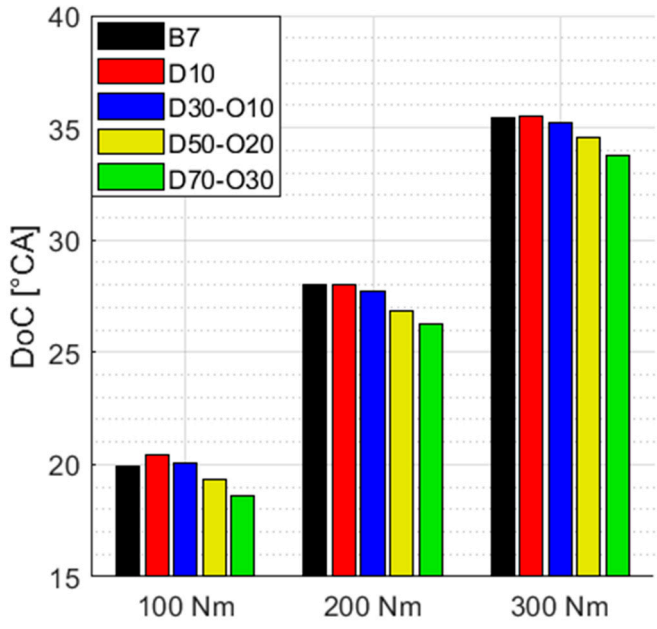

Figure 8. Duration of combustion of the tested fuels at 1400 rpm with different loads.

3.4.2. Heat Release Rates

Finally, the effects on the heat release rates were also investigated. For improved clarity, only the B7, D10, and D70-O30 blends are presented, and the curves for 200 Nm have been omitted, as they would not contribute any additional information. The in-between mixtures also had a similar behavior. Figure 9 demonstrates the heat release rates at 100 Nm. The combustion had a dominant premixed flame, and a slow but long diffusion phase occurred afterward. The combustion started similarly for all of the presented fuels. However, the length of the premixed phase was smaller for the blends with oxygenates. This meant that the premixed fuel burned faster due to the higher oxygen content. The shorter premixed phase could lead to a lower peak combustion pressure gradient, so these HRRs explain the results in Figure 6. The diffusion phase started earlier for the oxygenated fuels. It is discernible that D70-O30 had the highest HRR during the diffusion phase. This may be attributed to the mixture's high oxygen concentration and OME's high volatility.

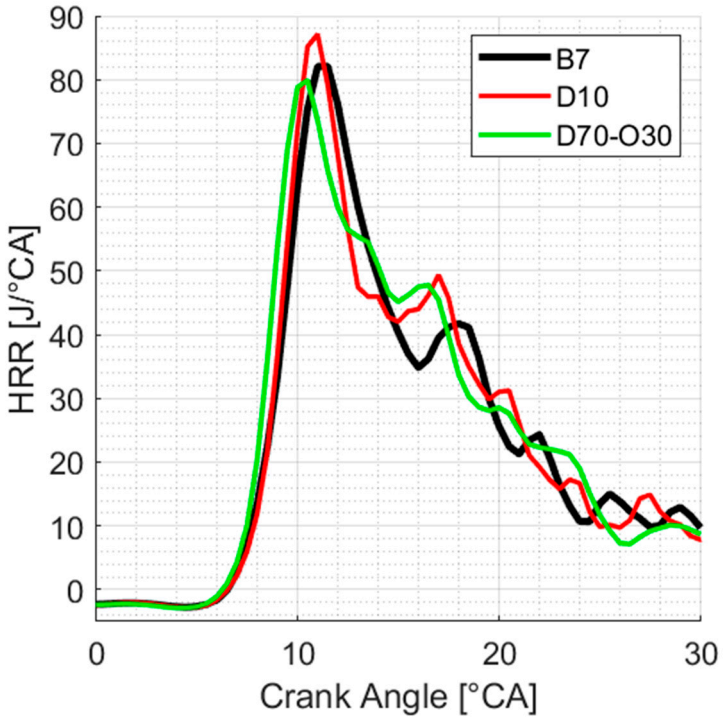

Figure 9. Heat release rates of the main blends at 1400 rpm and 100 Nm.

Figure 10 presents the heat release rates at 300 Nm. The combustion started with a premixed phase, but the following diffusion phase was dominant. The effects of OME and n-decanol on the premixed phase were similar to those in the 100 Nm case. D10 had a local HRR maximum that was similar to that of B7, and the premixed phase was finished earlier due to the higher oxygen concentration. However, D70-O30 had a lower local HRR maximum, so the advanced SoC presented in Figure 7 may have lowered the ID, resulting in a more heterogeneous mixture before combustion. D70-O30 had a much higher HRR when the diffusion flame started due to its high oxygen content. This faster start of the diffusion flame resulted in a shorter DoC, which led to a better BTE.

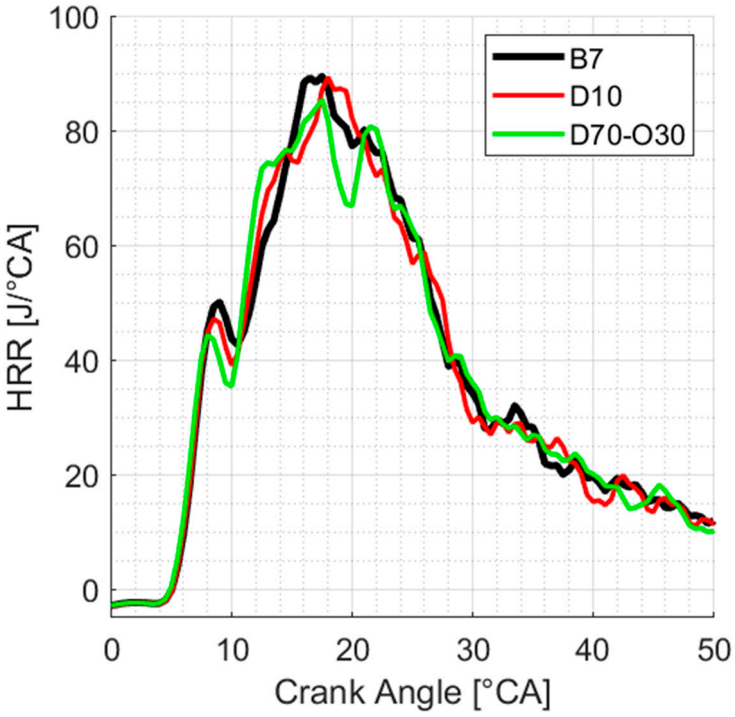

Figure 10. Heat release rates of the main blends at 1400 rpm and 300 Nm.

4. Conclusions

This study presented a new approach to enhancing the applicability of OME in compression ignition engines. By creating mixtures with n-decanol, blends close to the EN590 requirements could be created. The mixtures' six key properties and their compatibility with FKM sealings were investigated, and it was concluded that the fuels could be safely tested in an engine. Engine dyno tests were carried out at 1400 rpm with 100, 200, and 300 Nm loads, and the results related to emissions, economy, and combustion were presented.

The FKM compatibility assessment revealed that $OME_{3\text{-}5}$ resulted in major swelling of the sealings. The O-rings underwent unacceptable mass and volume increases of 56.69% and 106.38%, respectively, after 5 days of immersion in neat $OME_{3\text{-}5}$. The OME–decanol blends exhibited much less swelling, but durability tests should be performed to determine the long-term effects.

The engine dyno tests demonstrated that the applied oxygenates significantly improved the NO_x–PM trade-off compared to the B7 reference fuel. Among other aspects, the blends' high oxygen concentration can be identified as the main reason for this result. The high levels of oxygen in the fuel also improved the BTE. D70-O30 showed the highest increase, which was 7.6% at a high load. However, the smaller LHV may have decreased the fuel economy due to the higher BSFC. OME compensated for the lower cetane number of n-decanol to such an extent that certain blends exhibited cetane numbers even higher than B7's. This and OME's high volatility reduced the premixed flame phase, thereby decreasing the rate of increase in the peak pressure. However, the differences in the combustion were marginal when compared to the accuracy of the system, leading to the conclusion that the utilized blends exhibited similar combustion characteristics to those of conventional B7 diesel fuel.

Both OME and n-decanol can be created via climate-neutral methods; thus, they can be promising components of advanced fuel. The good NO_x–PM trade-off and BTE can contribute to the much cleaner operation of heavy-duty vehicles. Future works should investigate other parameters regulated by EN590, as well as the long-term effects on different alternative sealing materials and spray formations of the applied mixtures. Based on these results, new policies can later be formed for commercial vehicle manufacturers.

Author Contributions: Conceptualization, M.V. and M.Z.; methodology, M.V.; software, M.V.; validation, M.V.; formal analysis, M.V.; investigation, M.V.; resources, M.Z.; data curation, M.V.; writing—original draft preparation, M.V.; writing—review and editing, M.V.; visualization, M.V.; supervision, M.Z.; project administration, M.Z.; funding acquisition, M.Z. All authors have read and agreed to the published version of the manuscript.

Funding: This research was funded by the Hungarian Ministry of Innovation and Technology, KTI_KVIG_8-1_2021.

Data Availability Statement: The raw data supporting the conclusions of this article will be made available by the authors on request.

Acknowledgments: The research leading to these results was supported by AVL Hungary Kft. The authors are grateful for the OME_{3-5} research fuel and the analytical results provided by the Institute of Catalysis Research and Technology, Karlsruhe Institute of Technology. The authors express their gratitude to the researchers Ákos Bereczky and Dávid Csemány, Faculty of Mechanical Engineering, Budapest University of Technology and Economics, for their valuable professional advice and facilitation of the viscosity measurements. The authors are grateful to the researchers József Hlinka and László Dániel Erőss, Department of Automotive Technologies, Budapest University of Technology and Economics, for their support during the FKM compatibility assessments. The authors express their appreciation to László Horváth, a student in the Department of Automotive Technologies, Budapest University of Technology and Economics, for his assistance at the engine dyno laboratory.

Conflicts of Interest: The authors declare no conflicts of interest. The funders had no role in the design of the study, in the collection, analyses, or interpretation of data, in the writing of the manuscript, or in the decision to publish the results.

Abbreviations

BSFC: Brake Specific Fuel Consumption; BTE, Brake Thermal Efficiency; CN, Cetane Number; DME, Dimethyl Ether; DoC, Duration of Combustion; EGR, Exhaust Gas Recirculation; EU, European Union; HFRR, High-Frequency Reciprocating Rig; HP-EGR, High-Pressure Exhaust Gas Recirculation; HRR, Heat Release Rate; ICN, Indicated Cetane Number; ID, Ignition Delay; LHV, Lower Heating Value; LP-EGR, Low-Pressure Exhaust Gas Recirculation; NOx, Nitrogen Oxides; OME, Oxymethylen Ether; PM, Particulate Matter; SoC, Start of Combustion; WSD, Wear Scar Diameter; WTW, Well-to-Wheel.

References

1. Delbeke, J.; Runge-Metzger, A.; Slingenberg, V.; Werksman, J. *The Paris Agreement in Towards a Climate-Neutral Europe*, 1st ed.; Routledge: London, UK, 2019. [CrossRef]
2. Ovaere, M.; Proost, S. Cost-effective reduction of fossil energy use in the European transport sector: An assessment of the Fit for 55 Package. *Energy Policy* **2022**, *168*, 113085. [CrossRef]
3. eFuel Alliance: Press Release. 2022. Available online: https://www.efuel-alliance.eu/fileadmin/Downloads/E_PM_eFA_EU-Parlament_vor_Richtungsentscheidung_02062022.pdf (accessed on 10 December 2023).
4. Wu, F.; Fang, S.; Kuenzel, M.; Mullaliu, A.; Kim, J.K.; Gao, X.; Diemant, T.; Kim, G.-T.; Passerini, S. Dual-anion ionic liquid electrolyte enables stable Ni-rich cathodes in lithium-metal batteries. *Joule* **2021**, *5*, 2177–2194. [CrossRef]
5. Blakey, S.; Rauch, B.; Oldani, A.; Lee, T. Advanced Fuel Property Data Platform: Overview and Potential Applications. *Front. Energy Res.* **2022**, *10*, 771325. [CrossRef]
6. Fu, J.; Turn, S.Q. Characteristics and stability of biofuels used as a drop-in replacement for NATO marine diesel. *Fuel* **2019**, *236*, 516–524. [CrossRef]
7. Dhinesh, B.; Lalvani, J.I.J.; Parthasarathy, M.; Annamalai, K. An assessment on performance, emission and combustion characteristics of single cylinder diesel engine powered by Cymbopogon flexuosus biofuel. *Energy Convers. Manag.* **2016**, *117*, 466–474. [CrossRef]
8. Schmitz, R.; Russo, C.; Ferraro, F.; Apicella, B.; Hasse, C.; Sirignano, M. Effect of oxymethylene ether-2-3-4 (OME2-4) on soot particle formation and chemical features. *Fuel* **2022**, *324*, 124617. [CrossRef]
9. Prentice, I.C.; Farquhar, G.D.; Fasham, M.J.R.; Goulden, M.L.; Heimann, M.; Jaramillo, V.J.; Kheshgi, H.S.; Le Quéré, C.; Scholes, R.J.; Wallace, D.W.; et al. The carbon cycle and atmospheric carbon dioxide. In *Climate Change 2001: The Scientific Basis,*

Intergovernmental Panel on Climate Change. 2001, pp. 183–238. Available online: https://www.ipcc.ch/site/assets/uploads/2018/02/TAR-03.pdf (accessed on 12 December 2023).
10. Wicke, B.; Verweij, P.; Van Meijl, H.; Van Vuuren, D.P.; Faaij, A.P. Indirect land use change: Review of existing models and strategies for mitigation. *Biofuels* **2012**, *3*, 87–100. [CrossRef]
11. Bongartz, D.; Burre, J.; Mitsos, A. Production of Oxymethylene Dimethyl Ethers from Hydrogen and Carbon Dioxide Part I: Modeling and Analysis for OME1. *Ind. Eng. Chem. Res.* **2019**, *58*, 4881–4889. [CrossRef]
12. Cipriano, E.; da Silva Major, T.C.F.; Pessela, B.; Barros, A.A.C. Production of Anhydrous Ethyl Alcohol from the Hydrolysis and Alcoholic Fermentation of Corn Starch. *Cogn. Sustain.* **2022**, *1*. [CrossRef]
13. Alahmer, A.; Rezk, H.; Aladayleh, W.; Mostafa, A.O.; Abu-Zaid, M.; Alahmer, H.; Gomaa, M.R.; Alhussan, A.A.; Ghoniem, R.M. Modeling and Optimization of a Compression Ignition Engine Fueled with Biodiesel Blends for Performance Improvement. *Mathematics* **2022**, *10*, 420. [CrossRef]
14. Pali, H.S.; Sharma, A.; Kumar, M.; Annakodi, V.A.; Singh, N.K.; Singh, Y.; Balasubramanian, D.; Deepanraj, B.; Truong, T.H.; Nguyen, P.Q.P. Enhancement of combustion characteristics of waste cooking oil biodiesel using TiO_2 nanofluid blends through RSM. *Fuel* **2023**, *331*, 125681. [CrossRef]
15. Kowthaman, C.N.; Rahman, S.M.A.; Fattah, I.M.R. Exploring the Potential of Lignocellulosic Biomass-Derived Polyoxymethylene Dimethyl Ether as a Sustainable Fuel for Internal Combustion Engines. *Energies* **2023**, *16*, 4679. [CrossRef]
16. Härtl, M.; Seidenspinner, P.; Jacob, E.; Wachtmeister, G. Wachtmeister: Oxygenate screening on a heavy-duty diesel engine and emission characteristics of highly oxygenated oxymethylene ether fuel OME1. *Fuel* **2015**, *153*, 328–335. [CrossRef]
17. *BS EN 590:2022*; Automotive Fuels. Diesel. Requirements and Test Methods. European Committee for Standardization: Brussels, Belgium, 2023.
18. Agarwal, A.K.; Chandra, K. Di-ethyl ether-diesel blends fuelled off-road tractor engine: Part-I: Technical feasibility. *Fuel* **2022**, *308*, 121972. [CrossRef]
19. Virt, M.; Arnold, U. Effects of Oxymethylene Ether in a Commercial Diesel Engine. *Cogn. Sustain.* **2022**, *1*. [CrossRef]
20. Zhang, X.; Oyedun, A.O.; Kumar, A.; Oestreich, D.; Arnold, U.; Sauer, J. An optimized process design for oxymethylene ether production from woody-biomass-derived syngas. *Biomass Bioenergy* **2016**, *90*, 7–14. [CrossRef]
21. Debergh, P.; Gutiérrez-Sánchez, O.; Khan, M.N.; Birdja, Y.Y.; Pant, D.; Bulut, M. The Economics of Electrochemical Syngas Production via Direct Air Capture. *ACS Energy Lett.* **2023**, *8*, 3398–3403. [CrossRef]
22. Omari, A.; Heuser, B.; Pischinger, S.; Rüdinger, C. Potential of long-chain oxymethylene ether and oxymethylene ether-diesel blends for ultra-low emission engines. *Appl. Energy* **2019**, *239*, 1242–1249. [CrossRef]
23. Pélerin, D.; Gaukela, K.; Härtl, M.; Jacob, E.; Wachtmeister, G. Potentials to simplify the engine system using the alternative diesel fuels oxymethylene ether OME1 and OME3−6 on a heavy-duty engine. *Fuel* **2020**, *259*, 116231. [CrossRef]
24. Liu, J.; Wang, L.; Wang, P.; Sun, P.; Liu, H.; Meng, Z.; Zhang, L.; Ma, H. An overview of polyoxymethylene dimethyl ethers as alternative fuel for compression ignition engines. *Fuel* **2022**, *318*, 123582. [CrossRef]
25. Parravicini, M.; Barro, C.; Boulouchos, K. Experimental characterization of GTL, HVO, and OME based alternative fuels for diesel engines. *Fuel* **2021**, *292*, 120177. [CrossRef]
26. El-Seesy, A.I.; Xuan, T.; He, Z.; Hassan, H. Enhancement the combustion aspects of a CI engine working with Jatropha biodiesel/decanol/propanol ternary combinations. *Energy Convers. Manag.* **2020**, *226*, 113524. [CrossRef]
27. Nanthagopal, K.; Ashok, B.; Saravanan, B.; Pathy, M.R.; Sahil, G.; Ramesh, A.; Nabi, M.N.; Rasul, M.G. Study on decanol and Calophyllum Inophyllum biodiesel as ternary blends in CI engine. *Fuel* **2019**, *239*, 862–873. [CrossRef]
28. Preuß, J.; Munch, K.; Denbratt, I. Performance and emissions of long-chain alcohols as drop-in fuels for heavy duty compression ignition engines. *Fuel* **2018**, *216*, 890–897. [CrossRef]
29. Ashok, B.; Nanthagopal, K.; Darla, S.; Chyuan, O.H.; Ramesh, A.; Jacob, A.; Sahil, G.; Thiyagarajan, S.; Geo, V.E. Comparative assessment of hexanol and decanol as oxygenated additives with calophyllum inophyllum biodiesel. *Energy* **2019**, *173*, 494–510. [CrossRef]
30. Rajasekaran, S.; Damodharan, D.; Gopal, K.; Kumar, B.R.; De Poures, M.V. Collective influence of 1-decanol addition, injection pressure and EGR on diesel engine characteristics fueled with diesel/LDPE oil blends. *Fuel* **2020**, *277*, 118166. [CrossRef]
31. Hamilton-Kemp, T.; Newman, M.; Collins, R.; Elgaali, H.; Yu, K.; Archbold, D. Production of the Long-Chain Alcohols Octanol, Decanol, and Dodecanol by Escherichia coli. *Curr. Microbiol.* **2005**, *51*, 82–86. [CrossRef] [PubMed]
32. Rutter, C.D.; Rao, C.V. Production of 1-decanol by metabolically engineered *Yarrowia lipolytica*. *Metab. Eng.* **2016**, *38*, 139–147. [CrossRef]
33. Haltenort, P.; Hackbarth, K.; Oestreich, D.; Lautenschütz, L.; Arnold, U.; Sauer, J. Heterogeneously catalyzed synthesis of oxymethylene dimethyl ethers (OME) from dimethyl ether and trioxane. *Catal. Commun.* **2018**, *109*, 80–84. [CrossRef]
34. Csemány, D.; DarAli, O.; Rizvi, S.A.H.; Józsa, V. Comparison of volatility characteristics and temperature-dependent density, surface tension, and kinematic viscosity of n-butanol-diesel and ABE-diesel fuel blends. *Fuel* **2021**, *312*, 122909. [CrossRef]
35. *DIN EN 17155*; Liquid Petroleum Products—Determination of Indicated Cetane Number (ICN) of Middle Distillate Fuels—Primary Reference Fuels Calibration Method Using a Constant Volume Combustion Chamber. German Version; Deutsches Institut für Normung [DIN]: Berlin, Germany, 2018.
36. *ISO 12156 1*; Diesel Fuel Assessment of Lubricity Using the High-Frequency Reciprocating Rig (HFRR). International Organization for Standardization: Geneva, Switzerland, 2018.

37. *ASTM D 7094*; Standard Test Method for Flash Point by Modified Continuously Closed Cup (MCCCFP) Tester. ASTM International: West Conshohocken, PA, USA, 2013.
38. Virt, M.; Horváth, L.; Zöldy, M. Density and viscosity measurements for diesel-decanol-oxymethylene ether blends. *Angolan Miner. Oil Gas J.* **2023**, *4*, 1–5.
39. Nyerges, Á.; Zöldy, M. Verification and Comparison of Nine Exhaust Gas Recirculation Mass Flow Rate Estimation Methods. *Sensors* **2020**, *20*, 7291. [CrossRef]
40. Virt, M.; Granovitter, G.; Zöldy, M.; Bárdos, Á.; Nyerges, Á. Multipulse Ballistic Injection: A Novel Method for Improving Low Temperature Combustion with Early Injection Timings. *Energies* **2021**, *14*, 3727. [CrossRef]
41. Nyerges, Á.; Zöldy, M. Ranking of four dual loop EGR modes. *Cogn. Sustain.* **2023**, *2*. [CrossRef]
42. Heywood, J.B. *Internal Combustion Engine Fundamentals*; McGraw-Hill: New York, NY, USA, 1988.
43. Lakshminarayanan, P.A.; Aswin, S. *Estimation of Particulate Matter from Smoke, Oil Consumption and Fuel Sulphur*; SAE Technical Paper: Warrendale, PA, USA, 2016; p. 22016-32-0066.
44. Zeldovich, Y.B. The oxidation of nitrogen in combustion and explosions. *Acta Physicochem.* **1946**, *21*, 577–628.
45. Virt, M.; Zöldy, M. *The Effects of Oxygen from the Fuel and the Intake Air*; OGÉT; Hungarian Technical Scientific Society of Transylvania: Cluj, Romania, 2023.
46. Liu, J.; Sun, P.; Huang, H.; Meng, J.; Yao, X. Experimental investigation on performance, combustion and emission characteristics of a common-rail diesel engine fueled with polyoxymethylene dimethyl ethers-diesel blends. *Appl. Energy* **2017**, *202*, 527–536. [CrossRef]
47. Yin, X.; Li, Z.; Yang, B.; Sun, T.; Wang, Y.; Zeng, K. Experimental study of the combustion characteristics prediction model for a sensor-less closed-loop control in a heavy-duty NG engine. *Fuel* **2021**, *300*, 120945. [CrossRef]
48. Liu, H.; Wang, Z.; Zhang, J.; Wang, J.; Shuai, S. Study on combustion and emission characteristics of Polyoxymethylene Dimethyl Ethers/diesel blends in light-duty and heavy-duty diesel engines. *Appl. Energy* **2015**, *185*, 1393–1402. [CrossRef]